Experimental study of the fiber orientations in single and multi-ply continuous filament yarns

Aurélien Sibellas, Jérôme Adrien, Damien Durville, Éric Maire

Experimental Study of the Fibre Orientations in Single and Multi-ply Continuous Filament Yarns

Aurélien Sibellas[a,b,*], Jérôme Adrien[a], Damien Durville[b], Eric Maire[a]

[a] *Université de Lyon, INSA Lyon, MATEIS CNRS UMR5510, F-69621 Villeurbanne, France*
[b] *MSSMat Laboratory, CentraleSupélec, CNRS UMR8579, Université Paris-Saclay, F-91190 Gif-sur-Yvette, France*

Abstract

A detailed identification, using X-ray microtomography, of the filament trajectories within twisted single and multi-ply continuous filament yarns is presented in this article, in order to accurately determine the distributions of orientations of filaments which govern the mechanical behaviour of those yarns. The resolution of the images obtained by means of the X-ray microtomography experimental setup associated to the capabilities of an in-house developed image processing software allowed the reconstruction of the trajectories of almost all filaments within different yarn specimens. Various valuable information is derived from these trajectories, dealing in particular with the orientation of individual filaments with respect either to the ply trajectory or to the yarn axis. Compared to orientation distributions provided by different analytical models available in literature, those resulting from reconstructed trajectories show similar global trends, while providing more details in peripheral regions and regions close to contact zones between plies. Maps of radial and spatial distributions of orientations provide a comprehensive representation of how filaments are oriented within the plies, which gives valuable insight into the sources of nonlinearities in the mechanical behaviour of filament yarns.

This paper contains about 6300 words.

Keywords: Yarn, Fibre, Orientation distribution, Statistical properties, X-ray microcomputed tomography

1. Introduction

A large number of continuous polymer fibres can be twisted together to make filament yarns providing a good flexural and torsional flexibility for a high strength in the longitudinal direction. Such yarns are widely used as reinforcement in composite materials. The non-linear mechanical behaviour of this kind of structure is highly dependent on the arrangement of the fibres. Mechanics of twisted yarns made of textile fibres have been studied extensively in the last century [1, 2, 3, 4] but most of the models make an important simplifying assumption on the path that fibres follow using ideal helical [1], conical [5], doubly wound helical [6] or non-uniform epihelical [7] trajectories. They

*Corresponding Author
Email addresses: aurelien.sibellas@insa-lyon.fr (Aurélien Sibellas), jerome.adrien@insa-lyon.fr (Jérôme Adrien), damien.durville@centralesupelec.fr (Damien Durville), eric.maire@insa-lyon.fr (Eric Maire)

must be well-defined to derive their analytical deformation. Nevertheless, some authors developed an energy-based theory [2] allowing simpler calculations for the mechanical properties of the yarn. This theory was formulated in the form of Principle of Virtual Work by Leech [8]. This theory has been then improved to take into account complex geometries of fibre paths using orientation density functions [9, 10, 11, 12] that describe the distributions of angles formed by elementary segments of fibres with a given axis all over the structure. These orientation density functions (ODF) help representing both ideal and irregular structures which are used as input for mechanical models.

A few experiments were carried out in order to evaluate these orientations. First, to determine the path of the fibres, Morton and Yen [13] invented the Fibre Tracer Technique. A few coloured fibres were inserted in the original bundle. Once the yarn is twisted, it is immersed in a liquid of the same refractive index as the original fibres so that the coloured fibres can be observed under a standard optical microscope. This experiment remains the main technique used so far to characterize a few of the fibre trajectories. However, employing this technique, one has to assume that the parameters of the migration [14] (deviation from ideal path) are the same for all the other fibres which are not coloured. Although this technique is useful to estimate the magnitude of the migration, it can hardly provide a complete description of fibre trajectories that could be incorporated in mechanical models. Nevertheless, Lee and al. [15] used this experimental technique in order to get the orientation distribution of spun yarns from 420 tpm to 970 tpm and found that the frequency curves follow a normal law. To determine the complete distribution of fibre angle in the twisted yarn, Komori and Makishima[10] sliced thin microscopic sections perpendicular to the yarn axis which had been embedded at rest in a fixing material. Knowing the thickness of the slices (about 120 microns) and measuring the length of the fibre in them with a microscope, they could determine the distribution of fibre angles in the yarn. Like the previous experiment, the results show a distribution approaching a normal law. Only very few studies in the literature took this experimental procedure over. Instead, analytical models were developed to provide ODF describing the configuration of the fibre and even taking into account the radial migration of the fibres [16, 11, 12] but without accurate experimental support.

In this study, fibre trajectories in twisted yarns are investigated with a new method using X-ray micro-tomography at a resolution of 2.5 μm. Yarns are held with an in-situ tensile machine and scanned along 15 mm. Fibre paths are determined using image processing techniques implemented in a Matlab code. This leads to a complete numerical reconstruction of the studied yarn where each fibre trajectory is described by a set of spatial coordinates (x, y, z). Using these data, ODF could be calculated as well as maps of radial distributions of fibre orientations and maps of mean orientation in the yarn cross section for single and multi-ply yarns with different twist levels. These results allow to have a closer look in the inner structure of continuous-filament yarns.

2. Materials and Method

2.1. Materials

The bundles used before twisting are composed of 210 nylon fibres with an average diameter of 30 microns. The fibre bundles have a linear density of 140 tex (g/km) and are twisted using a ring spinning machine. Two steps of twisting are necessary to produce multi-ply yarns : each ply is first twisted (in direction z) independently to be combined in a cabled cord twisted in the opposite direction s during the second step. Continuous-filament yarns from one to three plies were made with an aimed twist of 230, 350 and 410 turns per metre (tpm). The aimed twist N_0 (the twist measured after twisting the yarn is between parenthesis), the diameter $d = 2r$ and the theoretical angle α at yarn surface ($\tan(\alpha) = 2\pi r N_0$) are summarized in table 1. Accurate values of yarn diameters were measured with a Z-Mike laser.

Table 1: Structural properties of the yarns studied. The aimed twist is followed between parenthesis, by the actual measured twist after twisting the yarns.

Type	Torsion (tr/m)	Diameter (mm)	α (°)
Single Yarn	230 (231)	0,48	9,2
	350 (355)	0,47	16,1
	410 (417)	0,48	23,9
Two-ply Yarn	230 (235)	0,71	27,7
	350 (348)	0,71	37,8
	410 (413)	0,72	43,1
Three-ply yarn	230 (228)	0,86	31,6
	350 (341)	0,9	44,0
	410 (407)	0,91	49,3

2.2. Experimental setup

X-ray microcomputed tomography is a non-destructive technique to obtain three-dimensional images of a sample at the microscopic scale [17]. It combines the information of many radiographs, each being taken at different angular steps of the sample in front of the detector. An in-situ tensile machine was especially developed in this study for the yarn prehension at rest (with a moderate applied load of 0.5 cN/tex) and for its extension. For the purpose of this article, only yarns at rest were analysed. This setup allowed a length of about 15 mm of each sample to be scanned which represents from 3 to 6 twist pitches for the different studied twist levels.

2.3. Determination of Fibre Trajectories

An *in-house* software is used to reconstruct fibre trajectories from images given by X-ray tomography. The sample being scanned along its longitudinal axis (z), (x, y) coordinates in slices perpendicular to the axis (fig. 1a) are used to track the fibres in the volume (fig. 1b). Each image is binarized and an algorithm identifies the centres of fibre cross-sections. Centres in successive planes are then associated using a proximity criterion to label 3D fibres and get their corresponding trajectories (fig. 1c). The curves are smoothed to remove spurious noise along the path. Usually, the trajectories of about 90% of the fibres can be entirely reconstructed by the software. The algorithm may fail to reconstruct the entire trajectory of a fibre along the scanned length when it is not able to determine the closest centre on the next slice or when cross-sections of fibres are too close to each other to be distinguished.

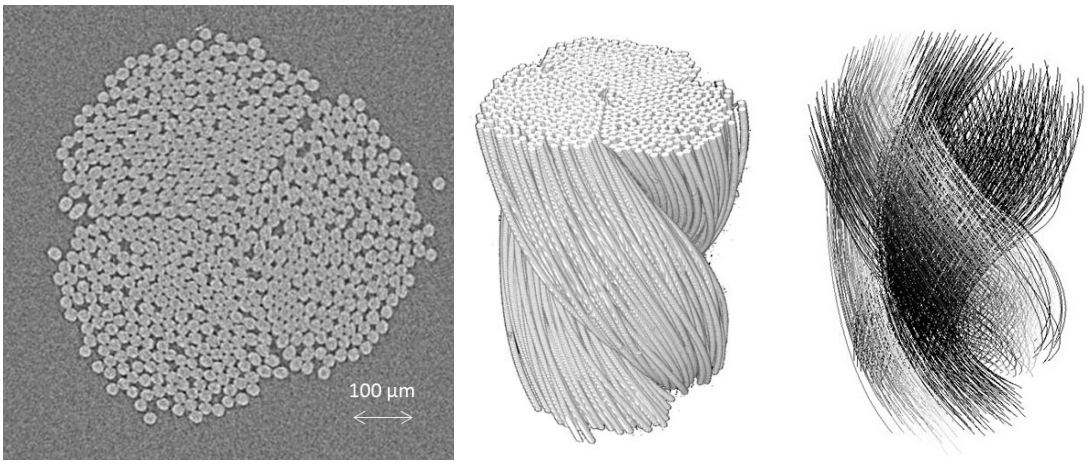

(a) (b) (c)

Figure 1: (a) Cross-section of 3-ply yarn obtained from X-ray microcomputed tomography. A stack of these images (perpendicular to the yarn axis) forms the 3D visualization on (b) and are used to track each fibre trajectory visible on (c) (length is about 2 mm).

3. Theoretical background

3.1. Definition

Fibre orientation is a key parameter for textile structures which has a major influence on the mechanical properties. It is defined as the angle between the unit tangent vector to the fibre path (or trajectory) and the yarn axis. In the case of yarns, the distribution of orientations results from the complex rearrangement of fibres induced by the twist, which is reflected by the phenomenon of migration. Two definitions of the orientation density function exist in the literature. The first defines the orientation vector in the unit sphere and derives the density function from the normalization conditions [10, 16, 18]. The second refers to the ratio between the cross-sectional area of fibres with a given angle

and the total cross-sectional area of fibres [11, 12]. Only the latter will be used in this study because of its physical meaning and the natural connection with the experimental results.

According to this definition, denoting $dA(\theta)$ the sum of cross-section area of fibres with an angle in the range [θ, $\theta + d\theta$], the orientation density function $\omega(\theta)$ is expressed as :

$$\omega(\theta)d\theta = \frac{dA(\theta)}{S_f} \tag{1}$$

where S_f is the sum of cross-sectional area of all fibres in the yarn. For axially symmetrical structures, knowing the expression of the orientation angle θ as a function of the distance ρ to the axis, or the expression of the reciprocal function $\rho(\theta)$, the orientation density function expresses as :

$$\omega(\theta) = \frac{2}{R^2}\rho(\theta)\frac{\partial\rho}{\partial\theta} \tag{2}$$

If the orientation angles are determined from measures, using the experimental relative frequency $P_{exp}(\theta, \Delta\theta)$ of orientation angles falling in the range [θ, $\theta + \Delta\theta$], the experimental orientation density function $\omega_{exp}(\theta)$ can be calculated with the relation :

$$\omega_{exp}(\theta) = \frac{P_{exp}(\theta, \Delta\theta)}{\Delta\theta} \tag{3}$$

3.2. Measurement of fibre orientation

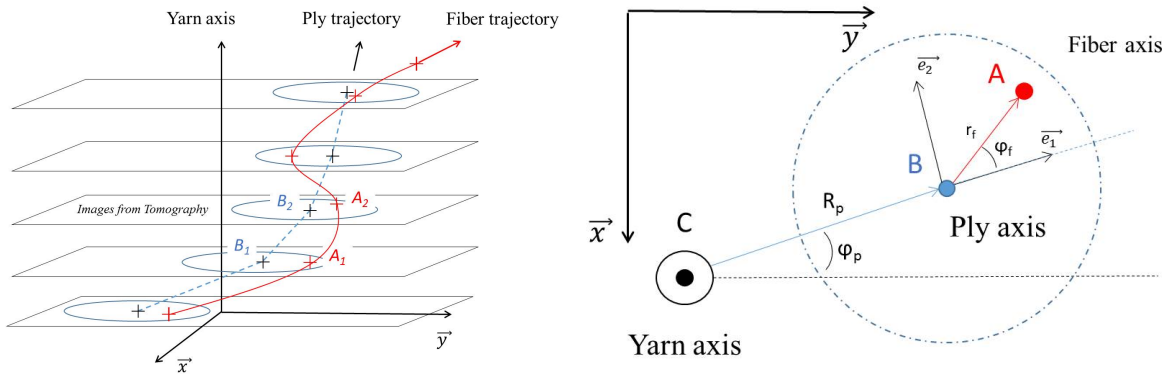

Figure 2: Definition of the yarn axis, the ply trajectory, the fibre trajectory and the geometric parameters.

Each fibre trajectory is defined as a series of segments delimited by spatial points A_i. Two successive points are spaced along the yarn by the size of a voxel (about 2.5 μm) determined by the resolution of the X-ray tomography. In single yarns, the fibre angle θ is calculated taking the arccosine of a dot product between each segment A_iA_{i+1} of the trajectory and the vertical axis ($\vec{z}$) :

$$\theta = \cos^{-1}\left[\frac{\overrightarrow{A_1A_2}.\vec{z}}{||\overrightarrow{A_1A_2}||||\vec{z}||}\right] \tag{4}$$

In multi-ply yarns, we can distinguish the fibre angle with respect to the yarn axis and another fibre angle with respect to the direction of the ply, defined as the tangent to the ply trajectory (see figure 2 for a description of these two

referentials). The ply trajectory is defined as a series of segments connecting the barycenters of the positions of the set of fibres from this ply in every image. This fibre angle θ for a segment is obtained with a dot product between this segment and the corresponding segment on the ply trajectory :

$$\theta = \cos^{-1}\left[\frac{\overrightarrow{A_1A_2}.\overrightarrow{B_1B_2}}{||\overrightarrow{A_1A_2}||||\overrightarrow{B_1B_2}||}\right] \tag{5}$$

The angles of fibres being determined for all 2D images from the tomography, the experimental relative frequency $P_{exp}(\theta)$ is calculated as the ratio between the number $n(\theta, d\theta)$ of fibre segments having their orientation falling into the range $\theta + \Delta\theta$ and the total number N_s of measured segments :

$$P_{exp}(\theta) = \frac{n(\theta, d\theta)}{N_s} \tag{6}$$

3.3. Mapping of the mean orientation angle

For a better understanding of the yarn inner structure, we study the spatial distributions of the mean fibre angles in the yarn cross-section. It means that for a specific point (x_i, y_i) located in the yarn cross-section, we get the mean angle of all fibres which have taken this position. These results can reveal either a pattern which comes from the twist and the process or a total blurred section due to a strong migration of the fibres and a widespread distribution of fibre orientations along the yarn axis.

The calculations of these spatial distributions are straightforward for single yarns where the yarn cross-section doesn't move in the global frame. The study for plies in multi-ply yarns has to be done in a local frame moving with the ply around the yarn axis. The right part of figure 2 shows a local frame $(\overrightarrow{e_1}, \overrightarrow{e_2})$, where $\overrightarrow{e_1}$ is defined as a unit vector with the direction $\overrightarrow{CB}$ and $\overrightarrow{e_2}$, a unit vector normal to $\overrightarrow{e_1}$. Each fibre segment has a set of local coordinates (x'_i, y'_i). As the frame is following the ply around the yarn axis, we can average the fibre angles which have the same position in the local coordinates. Because of the discrete nature of the results and the fibre position, we divide the ply cross-section in small squares (whose sides have a length of $1\mu m$) in which we calculate the orientation angles of fibres passing through.

3.4. Existing models

3.4.1. Single yarns

The simplest model for estimating the fibre distribution can be derived on the assumption of a linear variation of θ with the radial position ρ from 0 to the yarn surface angle α. Using equation 2, the following orientation density function is derived :

$$\omega(\theta) = \frac{2}{\alpha^2}\theta \tag{7}$$

where α can be calculated for a yarn with a radius R and a twist N_0 :

$$\tan(\alpha) = 2\pi R N_0 \tag{8}$$

Jeon and Lee [11] derived an orientation density function based on the model of perfect coaxial helices [1]. The relationship between θ and ρ is obtained from trigonometric considerations ($\tan(\theta) = 2\pi\rho N_0$) and leads to :

$$\omega(\theta) = \frac{2}{\tan^2(\alpha)} \tan(\theta) \sec^2(\theta) \tag{9}$$

Neckar and Das [18] created a unimodal model which describes the distribution of fibre orientations in a layer of a cylinder with a *preferential* orientation β :

$$u(\theta,\beta) = \frac{1}{\pi}\left[\frac{C}{C^2 - (C^2-1)\cos^2(\theta+\beta)}\right] + \frac{1}{\pi}\left[\frac{C}{C^2 - (C^2-1)\cos^2(\theta-\beta)}\right] \tag{10}$$

where C is a measure of the preferential modal direction. The authors considered a yarn as an assembly of concentric cylinders, each showing an orientation density function $u(\theta,\beta)$ where β depends on the distance from the yarn axis. This model was applied to a short staple yarn [19], assuming that the preferential angle β follows the standard model of coaxial helices ($\tan(\beta) = 2\pi r N_0$). In order to get the whole (marginal) orientation density function $\omega(\theta)$, one should integrate equation 10 from the centre of the yarn to its surface :

$$\omega(\theta) = \frac{2}{\tan^2(\alpha)} \int_0^{\alpha} u(\theta,\beta) \tan(\beta) \sec^2(\beta) d\beta \tag{11}$$

Figure 3a shows the different orientation density functions listed before for 3 values of the yarn surface angle α (10°, 30° and 50°). The figure 3b depicts Neckar's model (eq. 11) for 4 different values of C and $\alpha = 30°$. It can be seen that an increase of the value of C will sharpen the orientation density function around an angle a bit lower than the yarn surface angle α.

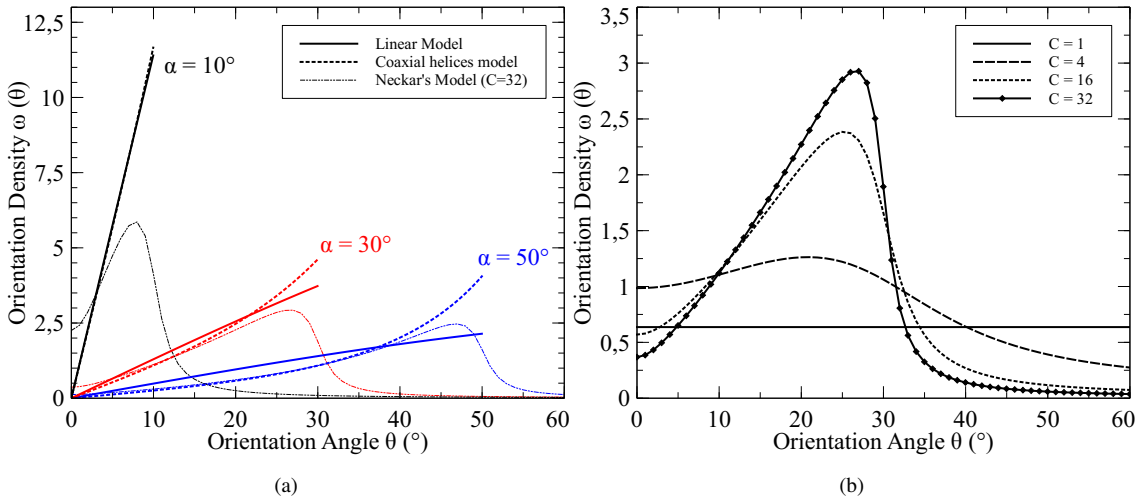

(a) (b)

Figure 3: (a) 3 models describe a distribution of fiber orientations in single yarn cross-sections (for 3 values of the yarn surface angle α) : the linear model (eq. 7), the perfect coaxial helices model (eq. 9) and Neckar's model (eq. 11). (b) Neckar's model for 4 values of C and a yarn surface angle $\alpha = 30°$.

3.4.2. Multi-ply yarns

Very few models describing fibre trajectories for multi-ply yarns can be found in the literature. Stansfield [7] developed a *non-uniform epihelix* which is a special case of Treloar's model [6] of a *doubly wound helix* where the ply cross-section can make an angle α with respect to the yarn axis. To determine the orientation density functions and the spatial maps of these angles, the expression of θ is given by Treloar (derived by Jeon and Kim [12] as well) as a function of the geometric parameters defining the parametric equations of the fibre trajectories. The main parameters are visible on the right part of figure 2. Here, α is the helix angle of the ply axis. θ is expressed as follows :

$$\theta(r_f, \phi_f) = \tan^{-1}\left[\frac{\sqrt{R_p^2 + (p^2 + \cos^2(\alpha))r_f^2 \sin^2(\phi_f) + (1 + p^2\cos^2(\alpha)r_f^2\cos^2(\phi_f) + 2R_p r_f(1 + p\cos(\alpha))\cos(\phi_f) + 2p\cos(\alpha)r_f^2}}{R_p\cot(\alpha) - p\sin(\alpha)\cos(\phi_f)}\right] \quad (12)$$

where p is defined in the relationship $\phi_f = p\phi_p$ and depends on the process parameters when the plies are twisted together. From the cording process of a multi-ply yarn, we know that each single yarn used will be untwisted of an amount equal to its original twist in the opposite direction of the cord twist. Theoretically, the value of p should be equal to -1 according to Jeon and Kim [12]. This value will be used in the following for comparisons between this model and experimental results.

4. Results and discussion

4.1. Effect of sample length and scanning location on the determination of the ODF

In order to examine the influence of scanned length on the orientation density function (ODF), ODF were determined for 5 different sample lengths on the same single yarn twisted at 410 tpm. The scanned lengths vary from 0.5 mm to 24.4 mm and the corresponding distributions are depicted in figure 4a. This shows that even with a minimum length of 0.5 mm, the yarn ODF is estimated with a fairly good accuracy. In the following, all samples have their ODF calculated over 15 mm. Then, to investigate the dependence of the determination of the ODF on the location of the scanned region of the sample, 2 different parts of 4.5 mm on the same yarn are scanned and analysed. The distributions remain close to each other (fig. 4b) which demonstrates the repeatability of the determination of the ODF along the sample.

4.2. Results

4.2.1. Single yarn

Orientation Density Functions. The ODF for the three single yarns (see table 1) are depicted in fig. 5d. Their shapes are very close to that of a normal law with a strong dependency on the twist. As expected, an increase of twist goes along with a shift to the right (towards higher angles) of the distributions. Besides keeping their shape, they become wider because of the number of higher angles induced by the twist. The three other figures (a, b and c) compare the experimental data with the models developed in the theoretical background part. In general, compared to a distribution based on the hypothesis of ideal coaxial helices or of uniform distribution, the first slope is in good agreement but

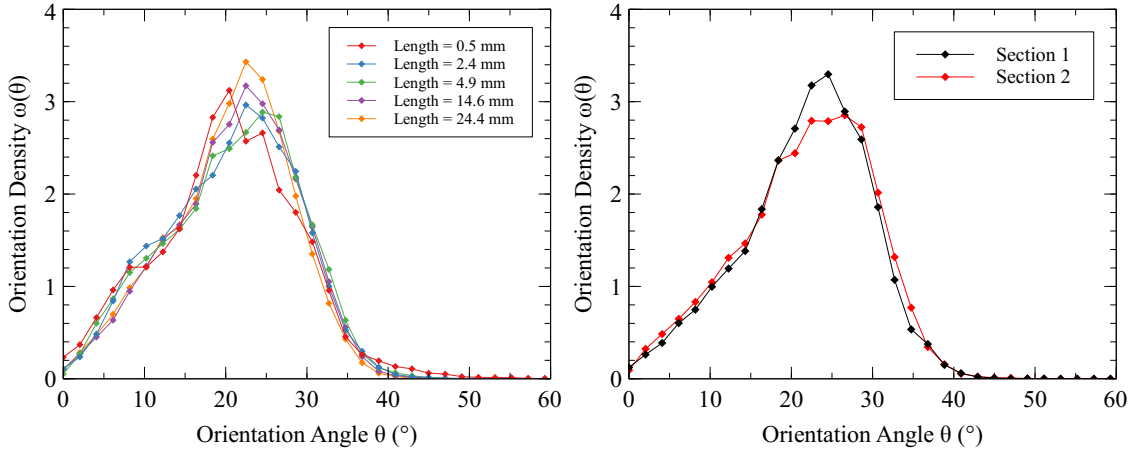

(a) (b)

Figure 4: (a) ODF of 5 different lengths (0.5 to 24.4 mm) of a single yarn (410 tpm) : the orientation density functions determined for these different size parameters of the sample show an independency of the location along the yarn axis and a relative accuracy of the measurements down to a length of 0.5 mm. (b) ODF of 2 different locations of a length of 4.5 mm in the same single yarn (410 tpm).

a discrepancy is observed for higher angles. Contrarily to Lee and al. [15] who considered that orientation angles followed a normal law for the staple yarns they studied, such an approximation by a normal law is not valid in our case, because of the higher experimental number of low angles leading to a non-symmetrical distribution. A better agreement is obtained with Neckar's model with a smooth decrease after reaching the main peak (at the surface angle) despite a discrepancy in the value of the peak (the value of C is chosen to give the best agreement).

Radial Distribution of Orientations. As previously shown, the global orientation density function is a way of describing the yarn structure but it hides the potential relationship between the orientation angle θ of a fibre segment and its relative radial position $\frac{r}{R}$ in the yarn section. To highlight this aspect, bivariate histograms showing the relative frequency of the two previous parameters combined are plotted in fig. 6. This representation gives an overview of the orientation distribution for each radial position in the yarn cross-section. About a few million fibre segments were used from the numerical data extracted with X-ray tomography to create these histograms. Note that the fibres can exceed a relative radial position greater than 1 because the value R_{yarn} of the yarn radius is measured with a specific set up (a laser Z-Mike) which provides the mean radius of the yarn. Furthermore, these bivariate histograms also show that the number of fibre segments decreases above a relative radial position of 0.8. This reflects the low radial packing density of fibres at the yarn surface.

Moreover, the orientation angles are not randomly distributed over the radial positions but they remain in a determined range (the vertical width of the coloured shape). The red curve on each figure describes the theoretical fibre angle according to the ideal coaxial helix model. In this model, the tangent of the angle is expressed linearly as a

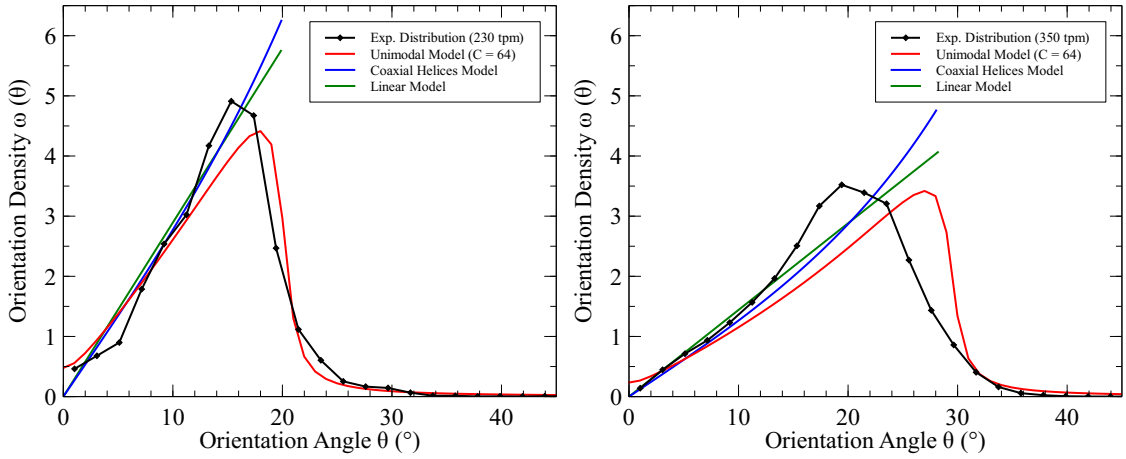

(a) N_0=230 tpm

(b) N_0=350 tpm

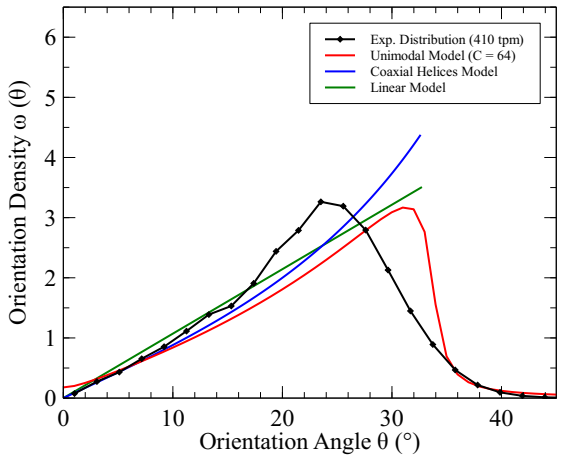

(c) N_0=410 tpm

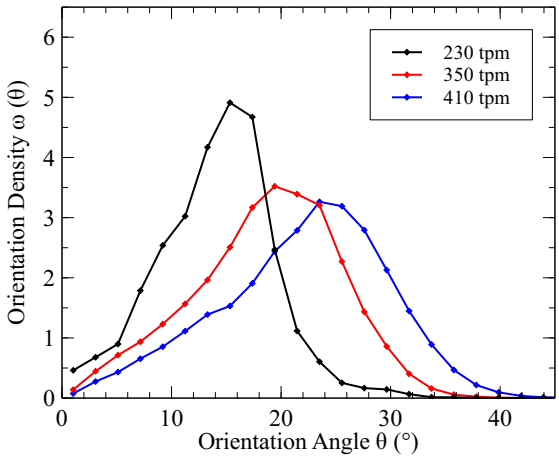

(d) Comparison of the 3 single yarns

Figure 5: (a, b, c) : Experimental orientation density functions of single yarns compared to existing models. (d) Comparison between the experimental ODF corresponding to the different twists.

function of the distance r to the axis and the twist N_0 ($tan(\theta) = 2\pi r N_0$). These figures demonstrate that the distribution of angles is globally centred on the values given by this model. In addition, several distributions of the fibre segments at a given radial position are plotted on figure 7 and show a good fit using normal laws.

Therefore, to build a realistic model of the single yarn structure, we can assume that the fibre orientations at a given radial position, follow a normal distribution centred on a preferential angle derived from the ideal coaxial helix model. Consequently, the orientation density function of a single yarn can be determined by replacing in equation 11 the term $u(\theta,\beta)$ by a normal law characterized by its standard deviation : σ is assumed to be fixed and depending on the structure (the mean value of σ in figure 7 is 0.065) and its mean value $\mu = \beta$ given by the model of coaxial helices.

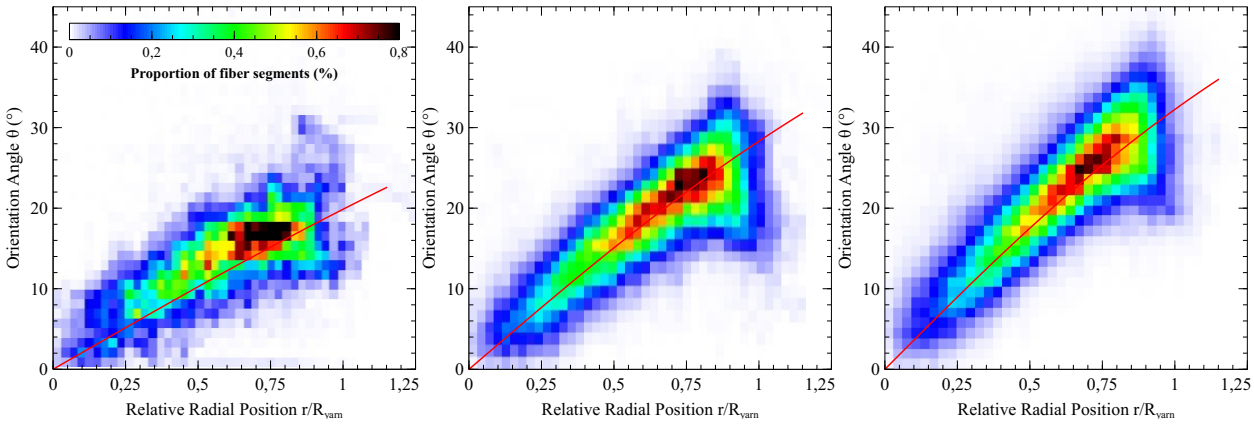

(a) N_0=230 tpm (b) N_0=350 tpm (c) N_0=410 tpm

Figure 6: Bivariate histograms of the orientation of fibre segments combined with their relative radial position in the single yarn cross-sections for 3 values of twist. The pattern indicates a preferential orientation which follows the relationship of ideal coaxial helices ($tan(\theta) = 2\pi \frac{r}{R} N_0$ which gives the red curves).

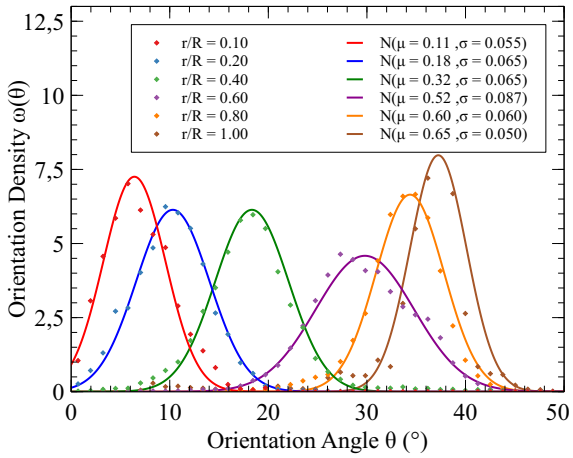

Figure 7: Distributions of orientations for different radial positions in a single yarn (N_0=410 tpm) and their approximation by fitted normal laws.

Spatial Distribution of Orientations. A single yarn cross-section is shown on fig. 8 on the right with its 3D volume on the left. Maps of mean orientation angles over this cross-section along the length of the samples are plotted in figure 9. It can be observed that fibre angles increase with the distance to the yarn axis. Moreover, the mean angle values at the centre are not equal to 0 but are slightly higher in every case and the angle values at yarn surface increases as the twist increases as it is expected.

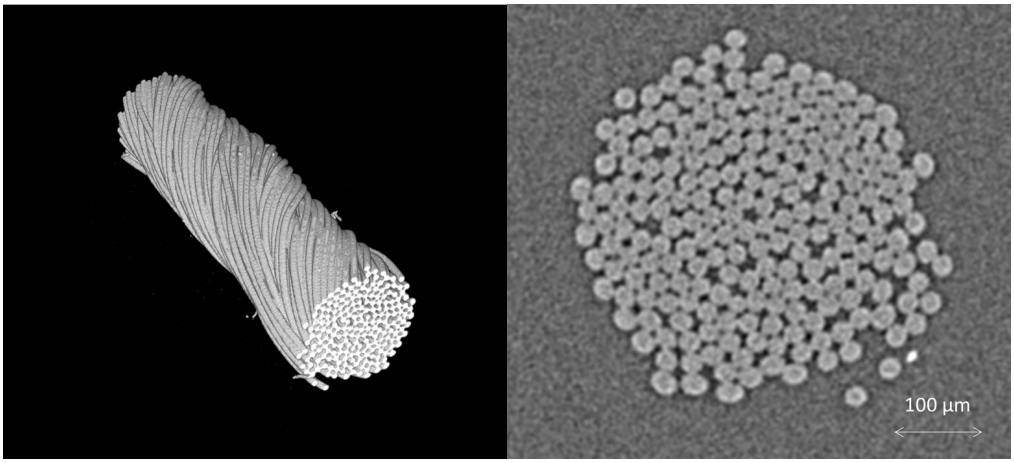

Figure 8: A 3D visualization of a single yarn (about 2 mm - 410 tpm) scanned with X-ray microtomography is shown on the left and one cross-section is shown on the right.

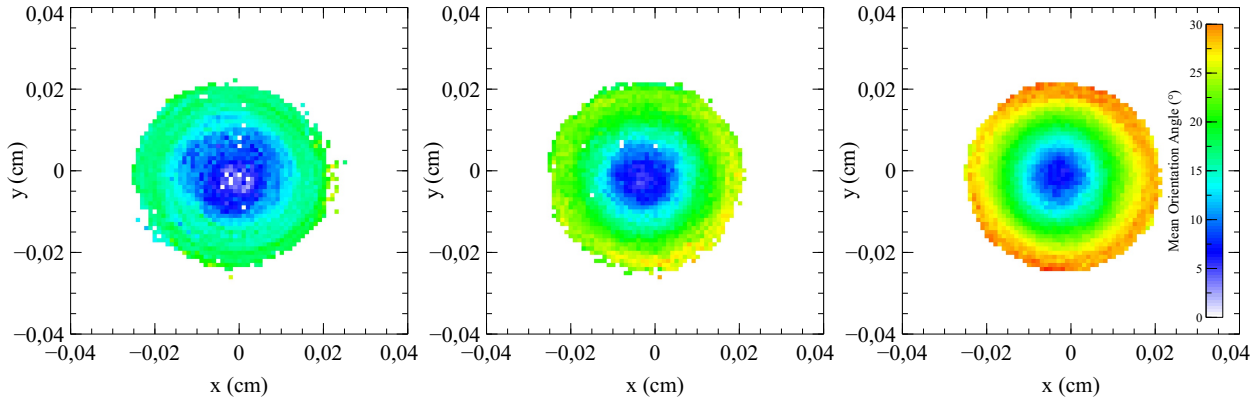

(a) N_0=230 tpm (b) N_0=350 tpm (c) N_0=410 tpm

Figure 9: Maps of mean orientation angles in single yarn cross-sections for different twist levels.

4.2.2. Two-ply yarn

Orientation Density Functions. The orientation density functions measured with respect to the yarn axis for 2-ply yarns are depicted on figure 10a with solid lines. The distributions are wider than the ones for single yarns and show a different shape displaying a first peak followed by a plateau or a smooth second peak for the most twisted yarns. In the same way, as the twist increases, the distribution is shifted to the right.

The twist of the single yarns before being assembled were equal (in opposite direction) to that of the final 2-ply yarn in which they are inserted. During the process, these single yarns are untwisted whereas the 2-ply yarn is twisted and hence, one would expect the plies to show a twist with respect to their axis (ply trajectory) quite close to 0 tpm and a sharp orientation distribution near 0°. These expected results are contradicted by the ODF displayed in 10b, which were calculated for each ply considering the orientation of each fibre with respect to the ply axis. This means that the arrangement of fibres within individual plies has been modified by the two stages of the twisting process. More importantly, by demonstrating that fibres within individual plies of a multi-ply yarn have a non-negligible orientation with respect to the ply trajectory, these experimental results indicate that the axial stiffness of these assembled plies should have a lower value than before twisting, because of the residual disorientation induced by the process. We know that the rigidity of a structure made of fibre depends on their orientation in comparison to the stress direction. In our case, this means that the mechanical behaviour of the plies under extension along their respective axis would be smoother than expected.

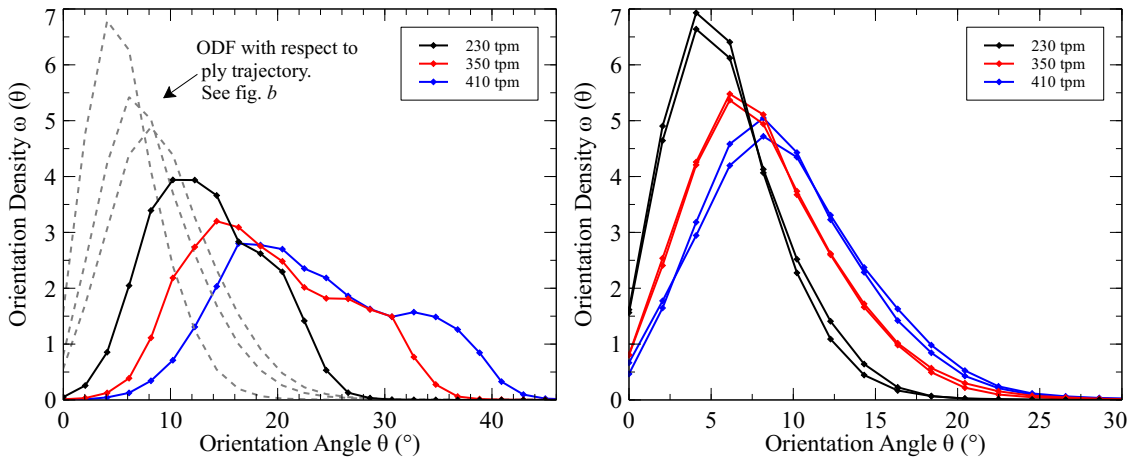

(a) ODF with respect to the yarn axis

(b) ODF with respect to the ply trajectories

Figure 10: (a) Impact of the twist level on the overall ODF of a 2-ply yarn with respect to the yarn axis (in solid lines). (b) For each level of twist, the ODF of each ply is reported independently with respect its corresponding ply trajectory. Due to the balanced cording process, the plies in the same 2-ply yarn show identical ODF.

Radial Distribution of Orientations. In order to understand more precisely the reasons for the shape of the distribution, the bivariate histogram of the orientation angles (with respect to the yarn axis) and the radial position of fibre segments is depicted in figure 11. It shows that the majority of orientation angles contributing to the first peak of the distribution comes from fibre segments having their relative radial position between 0.5 and 1. In addition, the highest orientation angles lie in general at a relative radial position below 0.5 where a combination of the nature of the trajectory and the contact between the plies modifies the orientation angles.

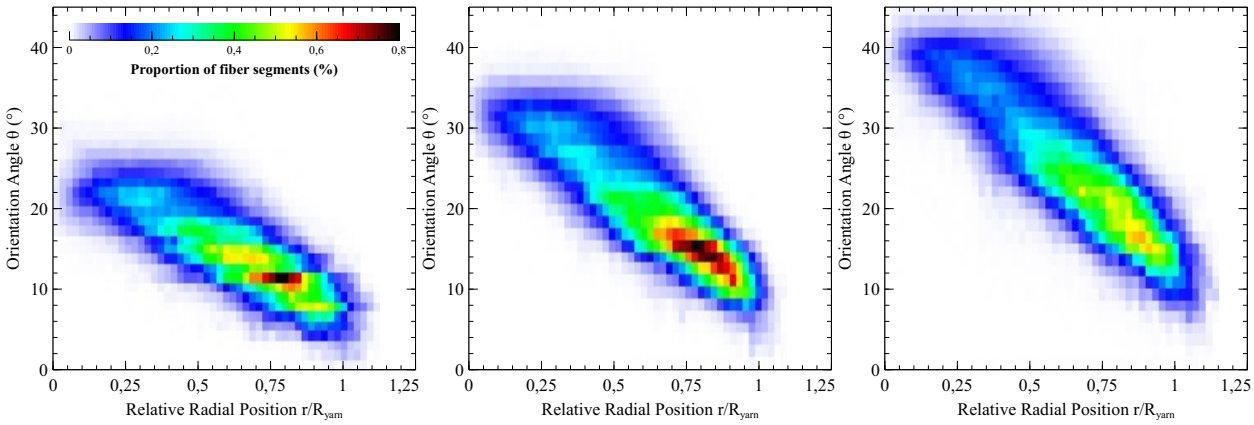

(a) N_0=230 tpm (b) N_0=350 tpm (c) N_0=410 tpm

Figure 11: Bivariate histograms of the orientation of fibre segments combined with their relative radial position in the 2-ply yarn cross-sections for 3 values of twist.

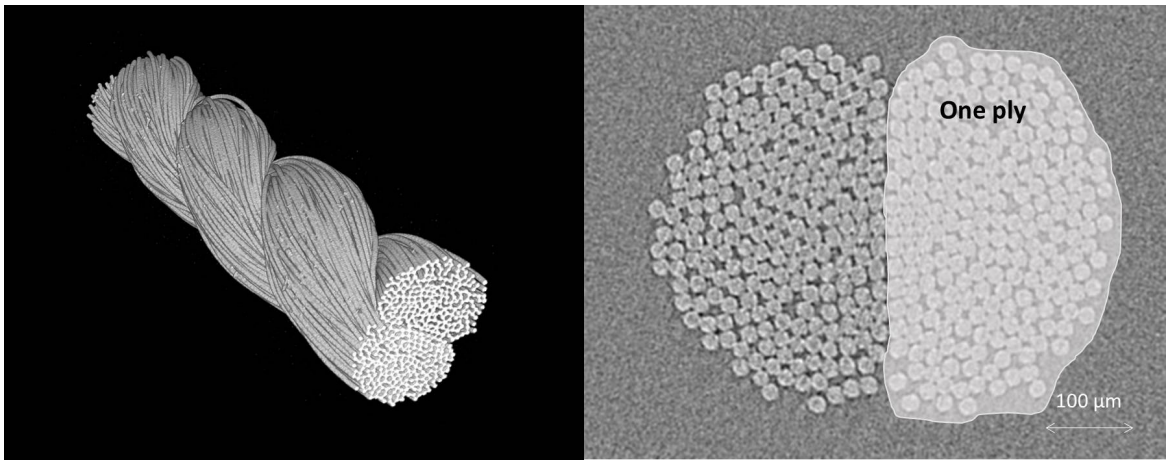

Figure 12: A 3D visualization of a 2-ply yarn (about 8 mm - 410 tpm) scanned with an X-ray microtomography is shown on the left and its cross-section is shown on the right.

Spatial Distribution of Orientations. A 3D volume of a 2-ply yarn obtained with an X-ray microtomography is given on fig. 12 whose cross-section is given on the right part of the figure which indicates the ply studied in the following. For 2-ply yarns, the spatial distribution of the fibre orientations of each ply is obtained in relation either to the yarn axis (fig. 13a, b and c) or to their corresponding ply trajectory (fig. 13d, e and f). These two points of view give a better understanding of the structure and lead a better comprehension of yarn micromechanics. First, with respect to the yarn axis, the highest angles are located close to the yarn axis, while the lowest angles are at the periphery of the yarn. However, examining the orientations with respect to the ply axis, lowest angles appear at the centre of the ply while highest are located near the flat contact zone between the plies.

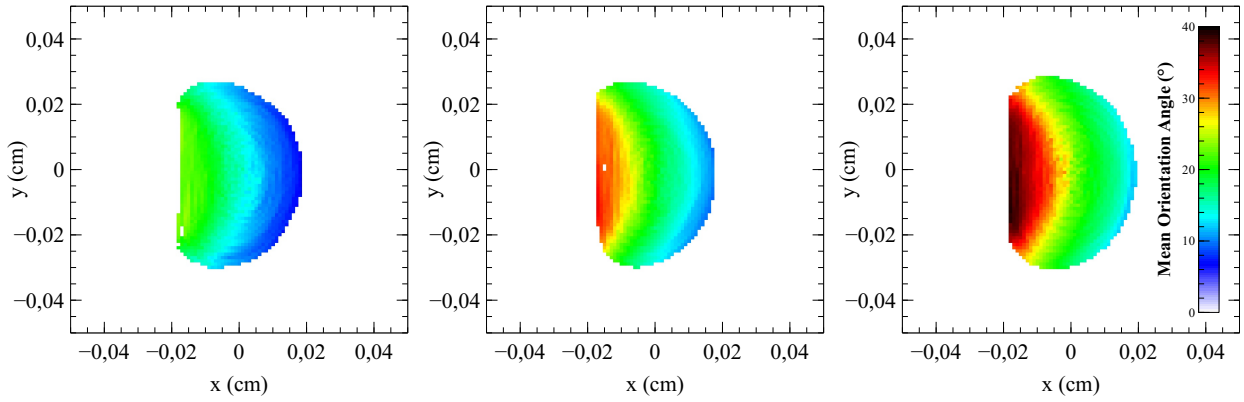

(a) N_0=230 tpm (b) N_0=350 tpm (c) N_0=410 tpm

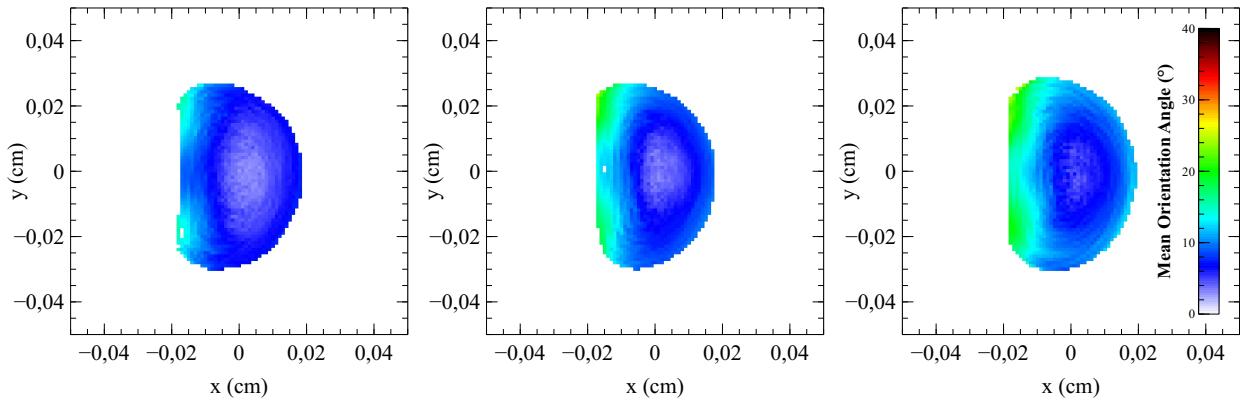

(d) N_0=230 tpm (e) N_0=350 tpm (f) N_0=410 tpm

Figure 13: (a, b, c) : Maps of the mean orientation angles in one ply of a 2-ply yarn (for different twist levels) with respect to yarn longitudinal axis. (d, e, f) : Maps of the mean orientation angles in the same ply with respect to its corresponding ply trajectory.

The theoretical spatial distribution of orientation angles is plotted in fig. 14a using equation 12 with a value of p equal to -1. The helix angle α of the plies with respect to the yarn axis is calculated using equation 8 with R estimated

on the images obtained from the X-ray tomography (R is the distance between the yarn axis and the ply axis). The map of the theoretical distribution of fibre angles shows that the highest angles are located at the centre of the yarn (in yellow) with a gradual decrease towards the periphery of the yarn (in green). Compared to the one derived from Treloar's model, the map of orientations obtained from experimental results (fig. 14b) shows a much larger range of measured orientations. This discrepancy highlights that the complex mechanisms of rearrangement taking place within the plies during the assembly process of the yarn induce a very specific distribution of angles that can hardly be taken into account by models only based on global twisting and untwisting effects at the scale of individual plies.

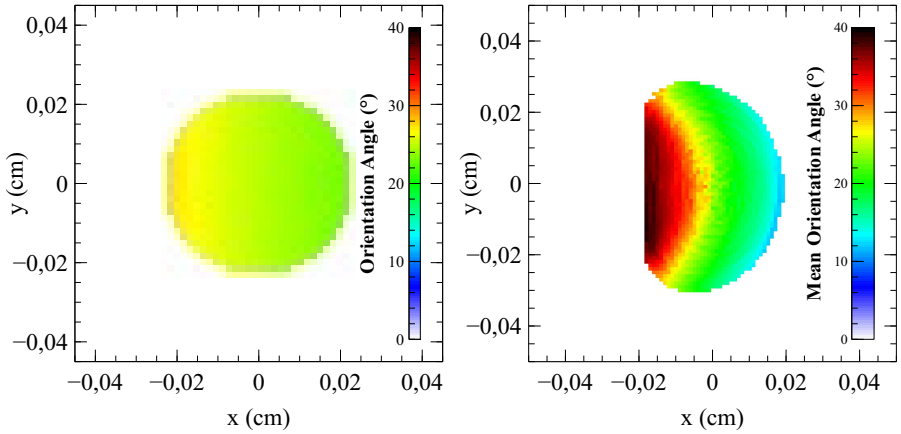

(a) N_0=410 tpm - Theoretical map

(b) N_0=410 tpm - Experimental map

Figure 14: (a) Theoretical (according to eq. 12) and (b) experimental spatial distribution of the mean orientation angles in a ply of a 2-ply yarn twisted at 410 tpm. The predicted angle values show a strong discrepancy.

4.2.3. Three-ply yarn

Orientation Density functions. ODF with respect to the yarn axis for 3-ply yarns are depicted in figure 15a with solid lines. They show a narrower distribution than the ones for 2-ply yarns and a shape close to a normal law. For the same reasons as those explained before, increasing the twist increases the fibre angles and shifts the whole distribution to the right, towards higher angles. The orientation distribution in each ply in the 3-ply yarns for each twist level with respect to the corresponding ply trajectory is depicted in figure 15b. For the same twist, these distributions are narrower and contains lower angles than those in the 2-ply yarns.

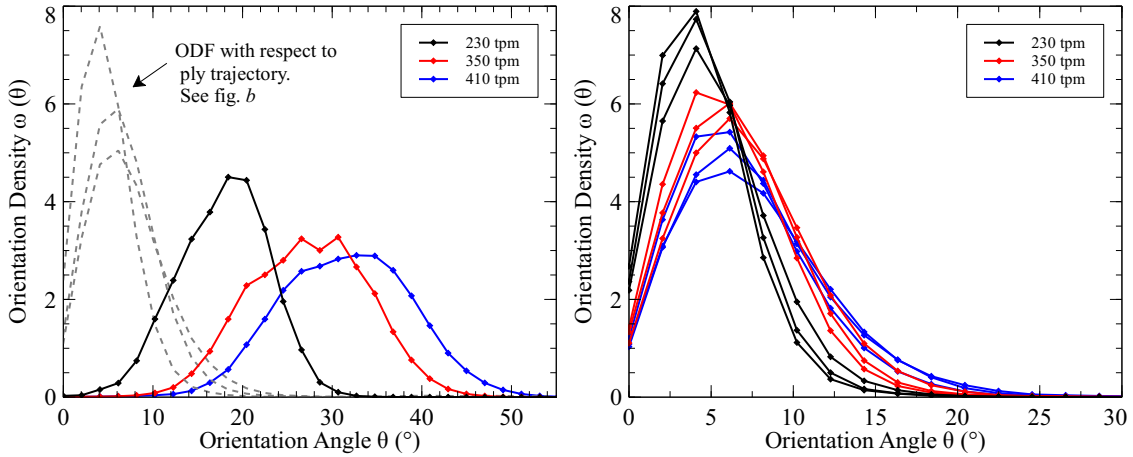

Figure 15: (a) Impact of the twist level on the overall ODF of a 3-ply yarn with respect to the yarn axis. (b) For each level of twist, the ODF of each ply is reported independently with respect its corresponding ply trajectory. Due to the balanced cording process like in the 2-ply yarns, the plies in the same 3-ply yarn show identical ODF.

Radial Distribution of Orientation. The radial distributions of the orientation angles are presented in figure 16. The global shape of these distributions is different from the ones of the 2-ply yarn. The evolution of the angle distribution is not monotonous with respect to the radial position, but shows a maximum value at a relative radial position of about 0.30. The triangular shape of the plies (fig. 1c) of the yarn may have a significant role in these discrepancies compared to 2-ply yarn. The 3-ply yarn is bigger than the 2-ply yarn made with identical bundles of fibres so the distance between the yarn axis and the ply axis will be higher, involving a higher helix angle of the ply axis for the same amount of twist. This can induce higher orientation angles along the fibre trajectories as it can be seen on the radial distribution.

Spatial Distribution of Orientation. The spatial distributions of the fibre orientations of each ply of 3-ply yarns (whose cross-sections are visible on fig. 1) are obtained in relation either to the yarn axis (fig. 17a, b and c) or to their corresponding ply trajectory (fig. 17d, e and f). Angle values with respect to the yarn axis are substantially higher than

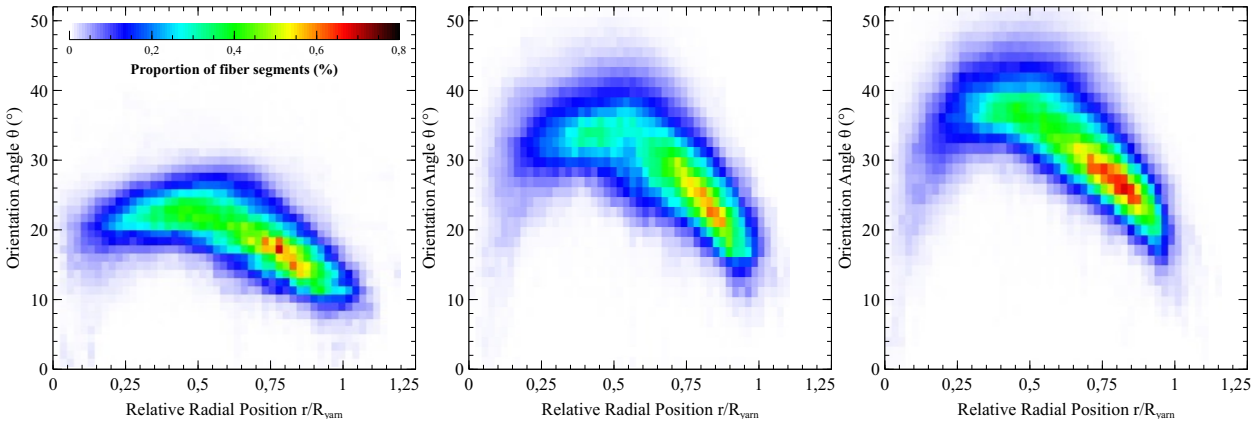

(a) N_0=230 tpm (b) N_0=350 tpm (c) N_0=410 tpm

Figure 16: Bivariate histograms of the orientation of fibre segments combined with their relative radial position in the 3-ply yarn cross-sections for 3 values of twist.

those in the 2-ply yarn whereas lowest angles are located either at the yarn surface or at the very centre of the yarn. The orientations with respect to the ply axis show the same pattern that exists in 2-ply yarns i.e. where the angles are small at the centre of the ply and increase until they reach their maximum value at the ply surface.

The map of theoretical orientation angles is depicted in figure 18. Like in 2-ply yarns, the range of measured orientation angles appears much larger than the one of angles determined by the theoretical model. The greater heterogeneity of the distribution of angles across the ply section observed in experimental results reflects the complexity of fibre trajectories within such yarns, and the difficulty to represent them through analytical models.

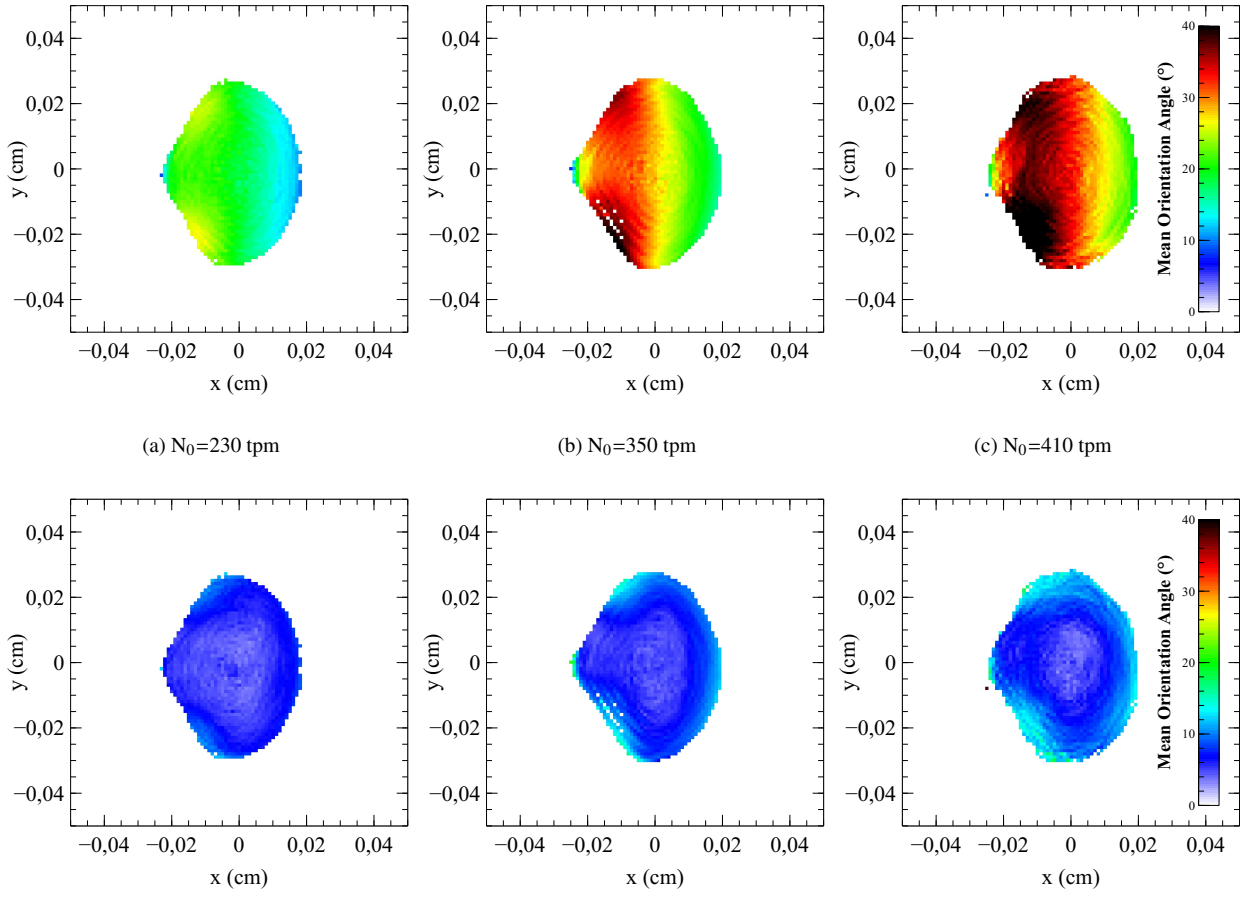

(a) N_0=230 tpm (b) N_0=350 tpm (c) N_0=410 tpm

(d) N_0=230 tpm (e) N_0=350 tpm (f) N_0=410 tpm

Figure 17: (a, b, c) : Maps of the mean orientation angles in one ply of a 3-ply yarn (for different twist levels) with respect to yarn longitudinal axis. (d, e, f) : Maps of the mean orientation angles in the same ply with respect to its corresponding ply trajectory.

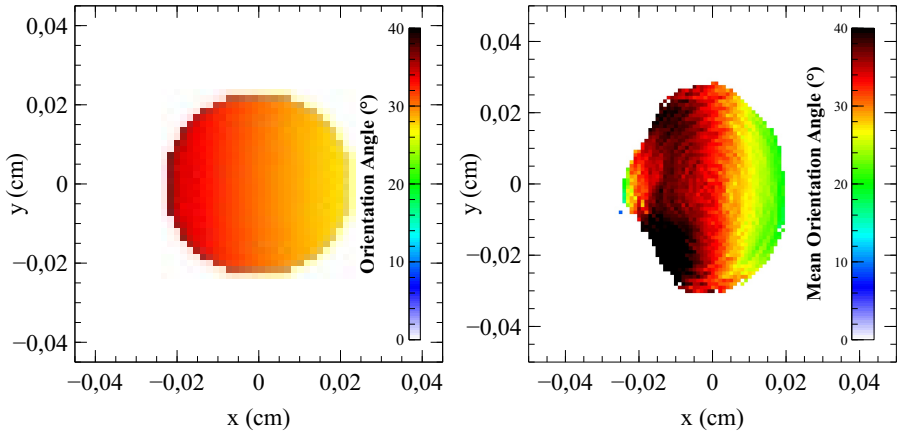

(a) N_0=410 tpm - Theoretical map

(b) N_0=410 tpm - Experimental map

Figure 18: (a) Theoretical (according to equation 12) and (b) experimental spatial distribution of the mean orientation angles in a ply of a 3-ply yarn twisted at 410 tpm. The predicted angle values also show a strong discrepancy.

5. Conclusions

Different specimens of single and multi-ply yarns (up to three plies) were scanned using an X-ray microtomography experimental set up with a resolution of 2.5 micrometres. Using image processing techniques, about 90% of the filament trajectories along 15 mm of each yarn could be reconstructed. Overall orientation density functions as well as maps of radial and spatial distribution of these orientations were derived from the reconstructed trajectories in order to have a better understanding of the inner structure of continuous-filament yarns. To the best of our knowledge, this is the first time that such a detailed description of the filament trajectories is provided. Compared to existing models in the literature, the orientation density functions resulting from reconstructed trajectories give access to more detailed descriptions, thus questioning the strong hypotheses on which these models are based. The orientation distributions with respect to the ply trajectory obtained for 2-ply and 3-ply yarns show a significantly wide range of orientations, thus highlighting the complexity of the rearrangement of filaments resulting from the stages of the twisting process. The proposed approach based on X-ray microtomography appears as a promising option to account for these complex mechanisms.

References

[1] J. Hearle, P. Grosberg, S. Backer, Structural Mechanics of Fibers, Yarns and Fabrics, Wiley-Interscience, New-York, 1969.

[2] L. Treloar, G. Riding, A theory of the stress-strain properties of continuous-filament yarns, Journal of the Textile Institute Transactions 54 (4) (1963) T156–T170. doi:10.1080/19447026308660166.

[3] N. Huang, G. Funk, Theory of Extension of Elastic Continuous Filament Yarns, Textile Research Journal 45 (1) (1975) 14–24. doi:10.1177/004051757504500103.

[4] J. Hearle, J. Thwaites, J. Amirbayat, Mechanics of dense fiber assemblies, in: Mechanics of Flexible Fibre Assemblies, Springer Netherlands, 1980, pp. 51–86.

[5] X. Tao, Mechanical Properties of a Migrating Fiber, Textile Research Journal 66 (12) (1996) 754–762. doi:10.1177/004051759606601203.

[6] L. Treloar, The geometry of multi-ply yarns, Journal of the Textile Institute Transactions 47 (6) (1956) T348–T368. doi:10.1080/19447027.1956.10750540.

[7] G. J. Stansfield, The geometry of twisted multi-filament structures, British Journal of Applied Physics 9 (3) (1958) 133–139.

[8] C. M. Leech, The modelling and analysis of the mechanics of ropes, Solid Mechanics and its Applications 209 (2014) 1–132. doi:10.1007/978-94-007-7841-2-1.

[9] J. Hearle, T. Sakai, On The Extended Theory of Mechanics of Twisted Yarns, Journal of the Textile Machinery Society of Japan 25 (3) (1979) 68–72.

[10] T. Komori, K. Makishima, M. Itoh, Mechanics of Large Deformation of Twisted-Filament Yarns, Textile Research Journal 50 (9) (1980) 548–555. doi:10.1177/004051758005000906.

[11] B. Jeon, J. Lee, A New Orientation Density Function of Ideally Migrating Fibers to Predict Yarn Mechanical Behavior, Textile Research Journal 70 (3) (2000) 210–216. doi:10.1177/004051750007000306.

[12] B. Jeon, Y. Kim, Orientation Density Function of Ply yarn, Textile Research Journal 80 (15) (2010) 1550–1556. doi:10.1177/0040517510363192.

[13] W. Morton, K. Yen, The arrangement of fibres in fibro yarns, Journal of the Textile Institute Transactions 43 (2) (1952) T60–T66. doi:10.1080/19447025208659646.

[14] J. Hearle, B. Gupta, V. Merchant, Migration of Fibers in Yarns: Part I: Characterization and Idealization of Migration Behavior, Textile Research Journal 35 (4) (1965) 329–334. doi:10.1177/004051756503500407.

[15] J. Lee, T. Gang, I. Park, A Study on the Geometrical Structure of Ring Spun Yarns, Textile Science and Engineering 26.

[16] N. Pan, Development of a Constitutive Theory for Short Fiber Yams: Part III: Effects of Fiber Orientation and Bending Deformation, Textile Research Journal 63 (10) (1993) 565–572. doi:10.1177/004051759306301002.

[17] E. Maire, J.-Y. Buffière, L. Salvo, J. Blandin, W. Ludwig, J. Létang, On the application of X-ray microtomography in the field of materials science, Advanced Engineering Materials 3 (8) (2001) 539–546.

[18] B. Neckář, D. Das, Modelling of fibre orientation in fibrous materials, Journal of the Textile Institute 103 (3) (2012) 330–340. doi:10.1080/00405000.2011.578357.

[19] B. Neckář, D. Das, Tensile behavior of staple fiber yarns part I: theoretical models, Journal of the Textile Institute 108 (6) (2017) 922–930. doi:10.1080/00405000.2016.1204899.